RSC Advances

PAPER

View Article Online
View Journal | View Issue

Cite this: *RSC Adv.*, 2025, **15**, 42614

The lysine degradation pathway analyzed with ^{1}H-NMR-targeted metabolomics of MG63 cells on poly(L-lactide)-based scaffolds

Zulka Ziblim,[a] Zhonglin Liu,[ab] Boontharika Thapsukhon,[c] Churdsak Jaikang,[de] Giatgong Konguthaithip,[de] Vachira Choommongkol,[f] Dheerawan Boonyawan[g] and Jetsada Ruangsuriya *[a]

A biomaterial is one of the key elements in tissue engineering, particularly for bone regeneration, as it withstands the human physiological environment and support essential cellular functions. Poly(L-lactide) (PLLA) is widely employed for biomedical applications, although there have been some drawbacks. We successfully developed PLLA composites using plasma-assisted and electrospinning methods. Conventional studies focus deeply on molecular interactions between cells and materials; however, studies aimed at understanding how cells metabolically respond to these materials have been limited. This work used ^{1}H-NMR-based metabolomics and multivariate statistical analysis to evaluate how PLLA composites metabolically guided MG63 osteoblast-like cells cultured on them. It was found that cells reacted uniquely on each scaffold type. PLS-DA suggested that succinic acid (2.39 ppm) and 3-hydroxy-L-proline (1.47 ppm) were the two metabolites with the highest variable importance in projection (VIP) values. Pathway enrichment analysis revealed that lysine degradation was considerably enriched (enrichment ratio: 2.0; $p < 0.05$). We further validated this prediction by supplementation with L-lysine at various concentrations, and it was confirmed that L-lysine supplementation significantly increased alkaline phosphatase activity, collagen synthesis, and mineralization, especially at 400 μM after 7 d. Consistent with this, the levels of lysine degradation intermediates were much lower on cellulose-containing scaffolds. These data suggest that activation of the lysine degradation pathway supports osteogenic activity.

Received 13th August 2025
Accepted 23rd October 2025

DOI: 10.1039/d5ra05954b

rsc.li/rsc-advances

1. Introduction

Biomaterials are some of the keystone elements in bone tissue engineering (BTE), which has emerged as a potential solution for bone repair and regeneration-related challenges. Many synthetic biomaterials have faced limitations when mimicking the complex architecture and biological functions of native bone, resulting in unsatisfactory rates of healing. Poly(L-lactide) (PLLA) has emerged as a widely used material in scaffold fabrication due to its biocompatibility, biodegradability, mechanical properties, ease of processing, and FDA approval. The biocompatibility of PLLA ensures minimal immune response, while its biodegradability allows for natural degradation into easily cleared products, such as lactic acid. Its processability enables the creation of films, fibers, and 3D scaffolds.[1–4] However, PLLA also presents limitations, such as its hydrophobicity, brittleness, relatively slow degradation rate, lack of inherent bioactivity, and potential for generating acidic degradation products.[1,5] To overcome these drawbacks and tailor PLLA for specific bone tissue engineering needs, researchers have explored various strategies.

Surface modification techniques have been utilized to enhance cell adhesion and proliferation. For instance, oxygen plasma treatment has been used to alter the surface properties of PLLA, making it more hydrophilic and promoting better cell attachment.[6,7] Additionally, coating PLLA with proteins, such as collagen, or polysaccharides, such as chitosan, was found to provide cell-binding sites and promote cell–matrix interactions, thereby improving cellular responses. In a previous study, melt-

[a]*Department of Biochemistry, Faculty of Medicine, Chiang Mai University, Chiang Mai 50200, Thailand. E-mail: jetsada.ruang@cmu.ac.th*
[b]*Center of Reproductive Medicine, Affiliated Hospital of Youjiang Medical University for Nationalities, Baise 533000, China*
[c]*Department of Chemistry, School of Science, University of Phayao, Phayao 56000, Thailand*
[d]*Department of Forensic Medicine, Faculty of Medicine, Chiang Mai University, Chiang Mai 50200, Thailand*
[e]*Metabolomic Research Group for Forensic Medicine and Toxicology, Department of Forensic Medicine, Faculty of Medicine, Chiang Mai University, Chiang Mai 50200, Thailand*
[f]*Department of Chemistry, Faculty of Science, Maejo University, Chiang Mai 50290, Thailand*
[g]*Department of Physics and Materials Science, Faculty of Science, Chiang Mai University, Chiang Mai 50200, Thailand*

spun aligned PLLA scaffolds coated with collagen enhanced osteoblast viability, adhesion, and directional migration, with collagen-coated scaffolds showing the greatest improvement in cell length and migration speed along the fiber axis.[8] Another strategy involves blending PLLA with other polymers to improve its overall properties. Combining PLLA with cellulose has been found to enhance the hydrophilicity and mechanical strength, creating a more favorable environment for cell growth. Previous studies have reported that PLLA reinforced with cellulose exhibited optimal performance, showing maximum crystallinity, thermal stability, mineralization, biodegradability, improved stiffness and mechanical properties, and enhanced polymer chain mobility.[9–12] Similarly, blending PLLA with collagen was reported to enhance cell adhesion, proliferation, and differentiation in yet another study,[6] as collagen provides cell-binding sites and promotes tissue regeneration. Furthermore, the incorporation of minerals like hydroxyapatite (HA) can improve the osteointegration of PLLA scaffolds, promoting better bone integration, as evidenced from a study where a PLLA/HA blend exhibited a significant decrease in the crystallinity of composite films compared to PLLA, and the presence of hydroxyapatite crystals did not have a significant influence on the degradation temperature of the composite films.[13]

Right after biomaterials are successfully fabricated, *in vitro* examinations of cellular responses are always conducted, primarily to ensure biocompatibility and cytotoxicity responses. Moreover, molecular observations are always carried out to deeply understand the biomaterial surface and cell interactions. For example, cell adhesion, proliferation, and protein expression (vinculin, Rac1, RhoA, and PCNA) were reported for MRC5 fibroblasts on PLLA films coated with fibronectin/laminin *versus* PLLA grafted with RGD/SIKVAV peptides. Western blot analysis revealed differences in vinculin, Rac1, and RhoA expression, indicating stronger mechano-transduction signaling on grafted surfaces, with RGD-grafted PLLA showing superior cell adhesion and proliferation compared to protein-coated PLLA.[14] In addition, researchers evaluated fibronectin/collagen-bonded poly(L-lactide-*co*-caprolactone) membranes *versus* unmodified polymers for esophageal cell cultures. The results revealed that fibronectin-modified PLLA promoted better collagen synthesis and cell proliferation and exhibited higher protein adsorption and enhanced mitochondrial activity in epithelial cells compared with the unmodified controls.[15] Mohammadalipour *et al.* found that adding cellulose nanofibers into electrospun polyhydroxybutyrate scaffolds greatly increased hydrophilicity, surface roughness, and degradation kinetics, all of which are important aspects relating to osteoblast activity. This study indicates that the incorporation of cellulose into scaffold matrices promotes superior cell adhesion and proliferation, primarily due to enhanced hydrophilicity and the presence of polar functional moieties, which are known to support protein adsorption and integrin receptor engagement.[10,12] While these conventional assays offer valuable information, a comprehensive understanding of scaffold–cell interactions also requires a deeper investigation into the metabolic changes occurring within cells during cell-biomaterial interactions. Moreover, there is limited data on how cell-biomaterial responses have been observed at the metabolome level. It would be worth exploring the metabolic changes of MG63 cells, a cell line generally used for bone tissue engineering studies, for primary observations.

Metabolomics is the study of metabolites under specific conditions and after specific durations. Metabolites are chemical products of cells, tissues, and/or organs responding to certain conditions and can be found in tissues and biological fluids, such as blood, plasma, serum, urine, and saliva. The applications of metabolomics in health and diseases are relatively new compared with other systems biology and omics fields, such as genomics, transcriptomics, and proteomics, which are used to reflect the state and severity of diseases, drugs, toxicity, and environmental effects.[16,17] The key steps of a metabolomics study are to separate and identify all the metabolites in each sample. Two main analytical platforms for metabolomics study are mass spectrometry (MS) and nuclear magnetic resonance spectroscopy (NMR).[18]

Focusing on bone tissue engineering, NMR metabolomics has emerged as a valuable tool for investigating the metabolic reprogramming of osteoblasts in response to different scaffold materials. For instance, NMR-based metabolomics has been used to study the metabolic response of human osteoblasts to non-poled and poled poly(L-lactic acid) (PLLA). The researchers found that osteoblasts cultured on PLLA scaffolds showed elevated lactate and a decrease in glucose, which indicated enhanced glycolysis and oxidative stress; activated TCA cycle intermediates (succinate), which suggested upregulated energy demand; and a decrease in storage lipids (triglycerides), implying membrane biosynthesis for cell growth.[19] In addition, metabolomics research into the development of bone disease treatment revealed metabolic shifts in cells exposed to hydroxyapatite (HA)-PLLA composites, including altered lipid profiles and energy metabolism. Arginine metabolism in macrophages (M1/M2 polarization) was also found to influence osteogenesis *via* nitric oxide (NO) pathways.[20] From all these studies, there remains a limited understanding of the dynamic metabolic responses of cells to fabricated biomaterials and the resulting changes in the metabolite microenvironment.

Therefore, the objective of this study was to utilize NMR spectroscopy to identify and quantify differential metabolites produced by MG63 cells cultured on various scaffolds we previously fabricated using PLLA-based polymers. Additionally, we aimed to analyze the relationship between the targeted metabolites and the metabolic pathways activated in response to MG63-cell interactions with the PLLA-based polymer. By addressing these objectives, this study aims to bridge the existing gap in knowledge relating to the field of BTE and to contribute to the development of more effective scaffolds that can enhance bone regeneration through a better understanding of cellular metabolism, ultimately contributing to the optimization of tissue engineering strategies.

2. Materials and methods

Poly(L-lactide) polymer (Ingeo 4043D), deuterium oxide (D_2O), 3-(trimethylsilyl)-2,2′,3,3′-tetradeuteropropionic acid (TSP), and L-

lysine monohydrochloride were purchased from Sigma-Aldrich (now MilliporeSigma; St. Louis, MO, USA). Microcrystalline cellulose was obtained from NatureWorks LLC. Fresh tilapia (*Oreochromis* spp.) skins were acquired from Mueang Mai Market in Chiang Mai province, Thailand, from which collagen was extracted and lyophilized in accordance with our previous study.[6]

2.1. Scaffold fabrication

Four types of scaffolds, including poly(L-lactide) (PLLA), PLLA-cellulose (PLLA-Cel), PLLA-collagen (PLLA-Col) and cellulose-PLLA-collagen (PLLA-Cel-Col), were fabricated using electrospinning and/or radio frequency (RF) oxygen plasma treatments in accordance with our previous research.[6] The Ingeo 4043D polymer (NatureWorks LLC, USA) used in this study has a number-average molecular weight (M_n) of 73 KDa with a dispersity index (Đ) of 1.5.[21] These molecular characteristics contribute to the mechanical properties and degradation profiles of the resulting scaffolds.

2.2. Cell seeding and NMR analysis

2.2.1. Seeding MG63 cells onto scaffolds. The MG63 osteosarcoma cell line (ATCC CRL1427, USA) was cultured in a sterile Nunc™ EasyFlask™ 75 (Thermo Fisher Scientific, China) using DMEM (Gibco®, USA) enriched with 10% fetal bovine serum (FBS), 2% HEPES buffer, 1% MEM non-essential amino acids (NEAAs), and 1% PenStrep (Gibco®, USA). Cultures were grown in a 5% CO_2 humidified incubator at 37 °C until 80–90% confluence. Cells were detached with 0.25% trypsin/EDTA (Gibco®, USA) for sub-culturing. For this study, MG63 cells from the 31st passage were used, seeded at 2×10^4 cells per mL in each well plate of a 6-well plate, with 3 replicates of each scaffold type. Prior to seeding with MG63 cells, the scaffolds were subjected to 15-minute UV sterilization, and the culture medium was changed every two days.

2.2.2. Extraction of metabolites. MG63 cells were cultured on each scaffold type for 7 d, and metabolites were extracted from the cells on each scaffold type using cell lysis buffer (CelLytic™ M, C2978-250 ML, Sigma-Aldrich, Saint Louis, MO, USA). Prior to extraction, the cell lysis buffer was aliquoted into a 15-mL tube and stored in a refrigerator at −80 °C for an hour. The cell medium was discarded, and the scaffolds were then cut into four quadrant pieces and transferred from the well plates to new 6-well plates. 1 milliliter (mL) of the precooled cell lysis buffer was then added to each scaffold quadrant piece, and they were transferred to the freezer at −80 °C to quench the cells and arrest further metabolism for a period of 20 min and thawed afterwards, before being aspirated into Eppendorf tubes.

The cell lysates in the Eppendorf tubes were subjected to 10-minute centrifugation at 14 000*g* (gravitational force) using a Beckman Coulter centrifuge (Allegra X-30R) at 4 °C. 950 μL of the supernatant was concentrated using a SpeedVac machine (Centrivap/Labconco, Kansas City, Missouri, USA) at 45 °C for 2 h, and the concentrates from each quadrant piece of the same scaffold replicate were pooled into one labelled Eppendorf tube. The pooled samples were dried further for another 2 h under the same conditions as the concentrates. The completely dried powdered samples were then stored in a freezer at −80 °C for further NMR processing.

2.2.3. NMR sample preparation and spectral acquisition. Metabolite extracts were reconstituted in 600 μL of 0.1 M TSP solution prepared in D_2O, containing 0.023 g of TSP per 100 mL of D_2O. This mixture was then centrifuged at 15 000*g* (gravitational force) for 5 min, and the supernatant was transferred into an NMR sample tube, capped, and labelled. The samples were taken for NMR metabolite analysis. ^{1}H NMR spectra were recorded using a Bruker AVANCE 500 MHz (Bruker, Bremen, Germany) instrument with a Carr–Purcell–Meiboom–Gill (CPMG, RD-90°, (t-180°), *n*-acquire) pulse sequence at 27 °C and water suppression pre-saturation. Key parameters are as follows: 16 scans, a 1-second relaxation delay, a 3.95-second acquisition time, an 8278.146-Hz spectral window, and a free induction decay (FID) resolution of 0.126 Hz with a 60.40 dwell time (DW), in accordance with a previous study.[22]

2.2.4. Quantification of metabolites from NMR spectra of obtained scaffolds. Based on previous research by Somtua *et al.*[22] with minor modifications, each metabolite was initially identified using the human metabolome database (HMDB, https://www.hmdb.ca). TSP served as an internal standard for quantifying metabolites. The peak acquisition and J-coupling values were analyzed using MestReNova (version 14.1.2-25024, MestreLab Research, Santiago de Compostela, Spain) software. The interpretation of NMR spectra of individual scaffolds was dependent on the use of chemical shift values. These values were important in identifying the signal for integration, calculating the integrated area, and estimating the coupling constant. To ensure accuracy, targeted metabolite peaks were identified, with a margin of error of 0.01 ppm, relative to the metabolite's resonances in the HMDB database. Representative spectral peaks for targeted metabolite quantification were selected based on signal intensities (as this made them more reliable and easier to detect); uniqueness (to avoid spectral overlaps); consistency of peaks; and diagnostic value relative to all other peaks. To quantify metabolites based on the representative peaks, the following formula was utilized:

$$C_{\text{met}} = \frac{I_{\text{met}} \times H_{\text{TSP}} \times C_{\text{TSP}}}{I_{\text{TSP}} \times H_{\text{met}}}$$

where C_{met}, I_{met}, H_{met}, C_{TSP}, I_{TSP}, and H_{TSP} are the concentration of metabolite, intensity of the metabolite, number of protons (H atoms) in the metabolite, concentration of TSP, intensity of TSP, and number of protons (H atoms) in TSP, respectively. Micromoles were used as the measurement unit for metabolite concentrations. While NMR-based metabolomics provides a robust, non-destructive approach for metabolite identification and relative quantification, it has inherent limitations in terms of absolute quantification precision compared to chromatographic methods.

For well-resolved peaks (*e.g.*, singlets like succinic acid at 2.39 ppm), integration was performed manually, and the error was 5–8% as a result of slight variations in integration. For overlapping peaks (*e.g.*, the multiplet for 3-hydroxy-L-proline at 1.47 ppm), we utilized the Global Spectral Deconvolution (GSD)

Table 1 Metabolite quantification in MG63 cells cultured on PLLA, PLLA-Cel, PLLA-Col, and PLLA-Cel-Col for 7 days. Metabolite concentrations (μM) are expressed as mean ± SD from 3 independent experiments ($n = 3$), and the coefficient of variation (CV) of each metabolite is calculated[a]

				PLLA ($n = 3$)		PLLA-Cel ($n = 3$)		PLLA-Col ($n = 3$)		PLLA-Cel-Col ($n = 3$)	
Metabolite	HMDB	Chemical shift (δ, ppm)	Multiplicity	Mean ± SD (μM)	CV (%)	Mean ± SD (μM)	CV (%)	Mean ± SD (μM)	CV (%)	Mean ± SD (μM)	CV (%)
Phosphoenolpyruvic acid	0000263	5.35	d	32.39 ± 1.81	5.59	14.14 ± 3.95	27.93	121.58 ± 67	55.11	0.97 ± 0.77	79.38
3-Phosphoglyceric acid	0000807	4.19	d	42.49 ± 24.17	56.88	6.18 ± 4.14	66.99	84.41 ± 61.66	73.05	1.79 ± 0.59	32.96
2-Phosphoglyceric acid	0000362	3.74	dd	160.75 ± 15.82	9.84	16.25 ± 10.74	66.09	176.43 ± 71.31	40.42	11.66 ± 8.5	72.9
5-Hydroxylysine	0000450	3.15	m	844.73 ± 279.07	33.04	19.1 ± 19.14	100.21	1379.05 ± 457.9	33.2	26.09 ± 32.14	123.19
Proline	0000162	2.99	d	791.39 ± 253.49	32.03	89.3 ± 49.67	55.62	1247.81 ± 687.4	55.09	63.09 ± 13.02	20.64
Pyruvic acid	0000243	2.36	s	390.2 ± 81.08	20.78	30.91 ± 12.17	39.37	563.94 ± 262.88	46.61	33.69 ± 15.8	46.9
Glycylproline	0000721	2.2	m	531.36 ± 132.63	24.96	51.52 ± 28.13	54.6	694.15 ± 234.29	33.75	37.29 ± 4.81	12.9
Lysine	0000182	2.12	m	149.25 ± 42.98	28.8	18.06 ± 13.1	72.54	161.32 ± 41.83	25.93	11.83 ± 3.35	28.32
Glucosylgalactosylhydroxylysine	0000585	1.92	m	114.14 ± 18.96	16.61	10.58 ± 5.78	54.63	159.52 ± 38.23	23.97	7.23 ± 1.67	23.1
3-Hydroxy-L-proline	0002113	1.47	m	178.15 ± 33.13	18.6	33.97 ± 12.36	36.39	394.53 ± 138.63	35.14	24.17 ± 7.3	30.2
Lactic acid	0000190	1.33	d	2126.55 ± 435.15	20.46	324.61 ± 150.41	46.34	4798.84 ± 2323.3	48.41	182.53 ± 105.35	57.72
NADH	0001487	8.16	s	25.28 ± 7.79	30.81	0.15 ± 0.07	46.67	58.06 ± 28.8	49.6	0.8 ± 1.01	126.25
cAMP	0000058	4.12	m	87.64 ± 16.55	18.88	14.21 ± 11.52	81.07	145.81 ± 82.11	56.31	5.63 ± 2.55	45.29
$FADH_2$	0001197	3.49	m	251.46 ± 30.91	12.29	24.67 ± 11.08	44.91	228.81 ± 105.22	45.99	17.12 ± 6.53	38.14
Acetyl-CoA	0001206	3.43	m	38.06 ± 11.42	30.01	52.5 ± 9.44	17.98	153.82 ± 173.67	112.9	3.63 ± 1.54	42.42
Oxaloacetic acid	0000223	3.33	s	467.28 ± 16.77	3.59	684.55 ± 98.86	14.44	857.72 ± 613.28	71.5	251.57 ± 302.01	120.05
α-Ketoglutaric acid	0000208	2.43	d	52.72 ± 14.22	26.97	12.24 ± 15.93	130.15	75.54 ± 29.58	39.16	3.81 ± 1.94	50.92
Succinic acid	0000254	2.39	s	31.67 ± 7.02	22.17	12.47 ± 13.85	111.07	166.65 ± 47.8	28.68	6.27 ± 2.59	41.31

[a] HMDB = human metabolome database; s = singlet; d = doublet; dd = doublet of doublets; m = multiplet.

algorithm in MestReNova. This process involves fitting a sum of Lorentzian line shapes to the experimental data. The fit was manually refined to minimize the residual. The integration error for these deconvoluted peaks, estimated from the variance of multiple fitting attempts, was 10–15%. The coefficients of variation (CV) reported in Table 1 reflect the combined effect of biological variability and analytical uncertainty, with higher CV values indicating either greater biological variation or increased analytical uncertainty due to signal overlap.

2.2.5. Multivariate and enrichment analysis of quantified metabolites. To gain insights into the complex dataset and to identify patterns and relationships derived from metabolite quantification that can serve as multidimensional features across different scaffold types, principal component analysis (PCA) and partial least-squares discriminant analysis (PLS-DA) were performed. MetaboAnalyst (version 6.0), a comprehensive web-based platform for metabolomic data analysis developed by the Xia Lab at McGill University (**https://www.metaboanalyst.ca**), was utilized for sample normalization, data transformation and scaling prior to the acquisition of PCA and PLS-DA statistical results.

Afterwards, enrichment analysis was conducted to understand the molecular basis behind the differential metabolite groupings found in multivariate analysis with the same MetaboAnalyst (version 6.0) tool. To obtain this data, the enrichment analysis module was used for sample normalization, data transformation and scaling. The Kyoto encyclopedia of genes and genomes (KEGG) metabolite library set of MetaboAnalyst version 6.0 was then used for data acquisition after data normalization.

2.2.6. Validation of metabolomics findings. Wet laboratory tests were designed to validate the suggested results from metabolic data. Biological activity assays were carried out using MG63 cells. Briefly, the cells were cultured with varied concentrations of L-lysine (0–400 μM) for 4 or 7 d, rinsed twice with phosphate-buffered saline (PBS) and incubated in 250 μL of CelLytic™ M cell lysis buffer (Sigma-Aldrich) for 20 min at room temperature after removing the culture medium. The lysates were harvested and stored at −20 °C for further analyses. L-lysine concentrations were selected based on physiological relevance and previous literature studies, where the physiological concentration of L-lysine in human blood is in the range of 100–300 μM,[23] with a maximum level of up to 400 μM observed in certain physiological states.[24] We selected three zones of concentrations to test whether the L-lysine concentration could affect bone formation. The first zone was 50 μM, which is below the normal physiological concentration; the second zone ranged between 100 and 300 μM, which are physiological concentrations; and the last zone was 400 μM, which is above the physiological concentration. In addition, previous *in vitro* studies successfully used a variety of L-lysine concentrations to stimulate bone-forming cells. For instance, concentrations up to 100 μM have been tested on rat bone marrow cells to assess osteogenic potential,[25] and higher concentrations have been used to successfully stimulate proliferation and matrix synthesis in human and rat osteoblasts.[26–28] Therefore, the 50–400 μM range is well-suited for investigating the enhancement of osteogenic markers in MG63 cells. The following bioactivities were determined.

2.2.6.1. Total protein determination. The Bradford assay was used to determine total protein in MG63 cell lysates. In brief, 20 μL of cell lysate was mixed with 200 μL of Bradford reagent (A6932, AppliChem), and the absorbance at 595 nm was measured after 10 min of incubation at room temperature (RT) using a microplate reader (Synergy S4; Biotek). Protein concentrations were determined using a bovine serum albumin (BSA) standard curve.

2.2.6.2. Collagen determination. Sirius Red staining was used to evaluate the collagen content. 50 μL of cell lysate was pipetted into a 96-well plate and allowed to dry at 60 °C for 3 h. 100 μL of prepared Sirius Red dye (Direct Red 80, Sigma-Aldrich) was then added to each well, and the plates were incubated for an hour. The unbound dye was subsequently washed with 0.05 M acetic acid. The collagen-bound dye was solubilized in 0.5 M NaOH, and the absorbance was recorded at 520 nm with a microplate reader (Synergy S4; Biotek). The collagen content in lysates was calibrated against a standard curve generated from tilapia skin collagen (5 mg mL^{-1}).[6]

2.2.6.3. ALP activity determination. ALP activity was measured based on the hydrolysis of *p*-nitrophenol phosphate. Briefly, 20 μL of lysate was combined with 80 μL of 1 mg mL^{-1} *p*-nitrophenol phosphate substrate (N2640, Sigma-Aldrich) in 1 M diethanolamine buffer (pH 9.8, D8885, Sigma-Aldrich) and incubated at 37 °C for 3 h. The reaction was stopped by the addition of 25 μL of 1 M NaOH, and the absorbance was measured at 405 nm with a microplate reader (Synergy S4; Biotek). ALP activity was determined based on a *p*-nitrophenol standard curve, and specific activity was normalized to the total protein amount in the lysate.

2.2.6.4. Mineralization determination. Mineralization was determined according to the method of Tsai *et al.*[29] with minor modifications. In brief, the cell layers with varied concentrations of L-lysine solution at days 4 and 7 were rinsed in PBS and fixed with 50% ethanol overnight at 4 °C. The fixative reagent was discarded, and the fixed sample was left to completely dry at RT. The cells were stained for 45 min at RT with 1 mL of 2% Alizarin Red S (pH 4.6) solution in each well. The dye was removed, and the stained layer was washed twice with distilled water to remove excess unstained dye. 250 μL of 10% (v/v) acetic acid was added to each well to re-solubilize the stained dye at RT for 30 min while shaking (Mini Rocker-Shaker, Biosan, Latvia). The absorbance of the resolubilized dye was measured at 450 nm with a microplate reader (Synergy S4; Biotek).

2.3. Statistical analysis

Data were analyzed using a multitiered statistical approach designed to ensure robust and reproducible insights into the metabolomics data. Prior to multivariate analysis, NMR spectral data underwent preprocessing, including binning into 0.04-ppm intervals from 0.00–8.5 ppm, with exclusion of the water region (4.6–5.0 ppm), normalization (auto scaling), and log-transformation to reduce heteroscedasticity. MetaboAnalyst (version 6.0) software was used to perform statistical analyses,

including principal component analysis (PCA) and partial least-squares discriminant analysis (PLS-DA) of metabolic groups between scaffold cohorts, with $p < 0.05$ indicating statistical significance. Data were analyzed using IBM SPSS Statistics 22 and R4.3.0 (https://cran.r-project.org/), and univariate analyses were performed using one-way ANOVA with Tukey's post-hoc test to determine statistically significant differences between experimental groups. Identification and quantification of metabolites were referenced in comparison to the HMDB, with 3-(trimethylsilyl)-2,2′,3,3′-tetradeuteropropionic acid (TSP) used as an internal standard for the purpose of normalization. Pathway enrichment analysis was conducted at a FDR < 0.05, and the top 25 enriched metabolic pathways and their enrichment ratios were obtained. Data are reported as mean ± standard deviation, and statistical significance is defined as $p < 0.05$.

3. Results

3.1 ^{1}H NMR spectra of MG63 cell metabolite profiles after culturing cells on different scaffold types

Using the human metabolome database (HMDB) as a reference standard, eighteen targeted metabolites of MG63 cells cultured on four scaffold types, including poly(L-lactide) (PLLA), PLLA-cellulose (PLLA-Cel), PLLA-collagen (PLLA-Col), and cellulose-PLLA-collagen (PLLA-Cel-Col), were characterized and quantified *via* ^{1}H NMR spectroscopy (Fig. 1). While the HMDB database assisted in the reliable identification of 18 targeted metabolites, several minor peaks remained unassigned because of signal overlap, residual solvent signals, or their absence from the database. This is a common limitation in untargeted metabolomics approaches, and our study focused on reliably identified metabolites with diagnostic value for bone tissue engineering applications. The identified peaks corresponding to the respective metabolites were selected and shown within the spectra. For example, lactic acid (1.33 ppm) showed fluctuating intensities over all types of scaffolds. Likewise, α-ketoglutaric acid (2.43 ppm), cAMP (4.11 ppm), and phosphoenolpyruvic acid (5.35 ppm) exhibited fluctuation. Extensive signal overlaps of resonances can be observed among the different stacked scaffold ^{1}H NMR spectra. The quantified metabolites and their coefficients of variations (CVs) were determined (Table 1).

Metabolite concentrations exhibited significant variations across the different scaffold types. For example, α-ketoglutaric acid from the cells on the PLLA-Cel scaffold exhibited the greatest variation (CV = 130.15%) followed by NADH on PLLA-

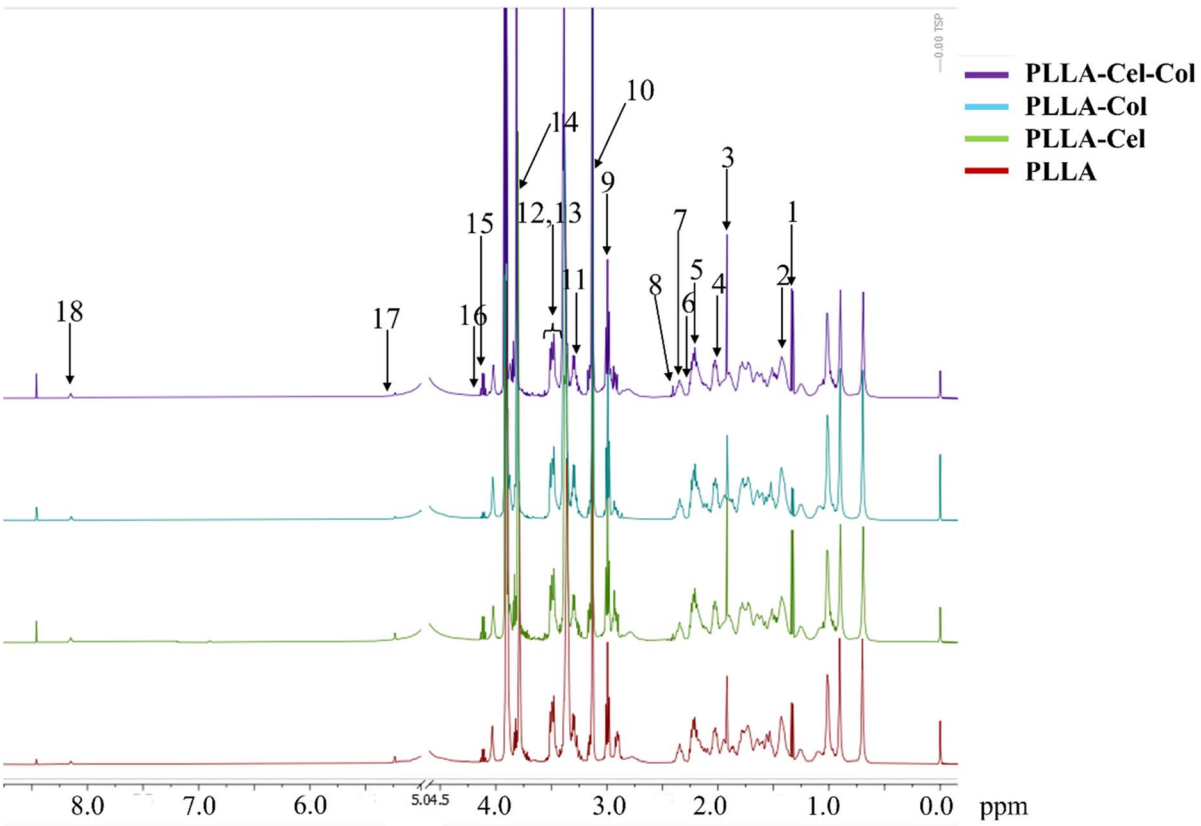

Fig. 1 Representative ^{1}H NMR spectra of MG63 cell metabolites after being cultured on different types of PLLA. The cells were seeded on PLLA, PLLA-Cel, PLLA-Col, and PLLA-Cel-Col for 7 days. Peak assignments: 1 – lactic acid, 2 – 3-hydroxy-L-proline, 3 – glucosylgalactosyl-hydroxylysine, 4 – lysine, 5 – glucosylproline, 6 – pyruvic acid, 7 – succinic acid, 8 – α-ketoglutaric acid, 9 – proline, 10 – 5-hydroxylysine, 11 – oxaloacetic acid, 12 – acetyl-CoA, 13 – $FADH_2$, 14 – 2-phosphoglyceric acid, 15 – cAMP, 16 – 3-phosphoglyceric acid, 17 – phosphoenolpyruvic acid, 18 – NADH. Unassigned peaks represent unknown compounds not in the HMDB database, residual solvent signals, or overlapping signals. The water signal region (4.6–5.0 ppm) was excluded from analysis to minimize interference.

Cel-Col (CV = 126.25%). 5-Hydroxy lysine showed elevated CVs on the PLLA-Cel and PLLA-Cel-Col scaffolds. Lactic acid demonstrates increasing CV values from PLLA to PLLA-Cel-Col. In contrast, differential metabolites associated with the pure PLLA scaffolds generally exhibited lower CV values. This differential metabolite variability reflects the plasticity of cellular metabolism under different material conditions.

3.2. Multivariate analysis of differential metabolites on different scaffold types

Principal component analysis (PCA) was primarily used to investigate differential metabolic heterogeneity among MG63 cells seeded on different types of PLLA. The PCA scores plot indicated that the sample groups were naturally separated by scaffold type, with the first two principal components, PC1 and PC2, accounting for 31.6% and 18.5% of the total differential metabolite variances, respectively (Fig. 2A). PC1 demonstrated the greatest separation between PLLA and the other composite scaffolds, which reflects the most significant metabolic change caused by the presence or absence of bioactive additives. PC2 improved resolution by discriminating between certain composite scaffolds, such as PLLA-Cel and PLLA-Col. The confidence ellipses surrounding each group indicated varied levels of within-group variability, with PLLA having larger dispersion than the other composites. However, statistical insignificance was observed after pairwise permutational multivariate analysis of variance (PERMANOVA) was performed on the PCA scores (Table 2).

To better elucidate the potential differential metabolites among the different scaffold groups, partial least-squares discriminant analysis (PLS-DA) was carried out. The PLS-DA scores plot (Fig. 2B) displayed the first two latent variables (Component 1 and Component 2), which together explained a significant portion of the variance related to group separation without outliers observed in the plot. Component 1 (21.7%) differentiated between PLLA and other scaffolds (PLLA-Cel, PLLA-Col, and PLLA-Cel-Col). This suggests that Component 1 captures the primary metabolic differences related to the presence or absence of bioactive additives (cellulose and/or collagen). Component 2 (21.8%) further separates the groups, particularly distinguishing PLLA-Cel from PLLA-Col and PLLA-Cel-Col.

Table 2 Pairwise permutational multivariate analysis of variance (PERMANOVA) results for PCA group comparisons. MG63 cells were cultured on PLLA, PLLA-Cel, PLLA-Col, and PLLA-Cel-Col for 7 days

Comparison	F. Model	R^2	*p*-val.	p. adj.
PLLA *vs.* PLLA-Cel	7.9269	0.66462	0.1	0.2
PLLA *vs.* PLLA-Cel-Col	3.2507	0.44833	0.2	0.3
PLLA *vs.* PLLA-Col	0.30047	0.06987	0.7	0.7
PLLA-Cel *vs.* PLLA-Cel-Col	7.6049	0.65532	0.1	0.2
PLLA-Cel *vs.* PLLA-Col	9.8215	0.7106	0.1	0.2
PLLA-Cel-Col *vs.* PLLA-Col	2.0856	0.34271	0.4	0.48

PLS-DA variable importance in projection (VIP) analysis was also calculated and further highlighted significant metabolites that drive scaffold group differentiation, with succinic acid (VIP = 2.3653, Component 1), 3-hydroxy-L-proline (VIP = 2.0326), lactic acid (VIP = 1.5342), proline (VIP = 1.0615), and glucosylgalactosylhydroxylysine (VIP = 1.0605) appearing as major contributors (Table 3).

3.3. Pathway enrichment analysis of metabolites from MG63 cells cultured on PLLA, PLLA-Cel, PLLA-Col, and PLLA-Cel-Col for 7 days

To elucidate the biological mechanisms underlying the distinct metabolite clustering observed in multivariate analyses, pathway enrichment analyses were undertaken (Fig. 3). It was found that two parallel pathways, D-amino acid metabolism and lysine degradation, were suggested, having the highest

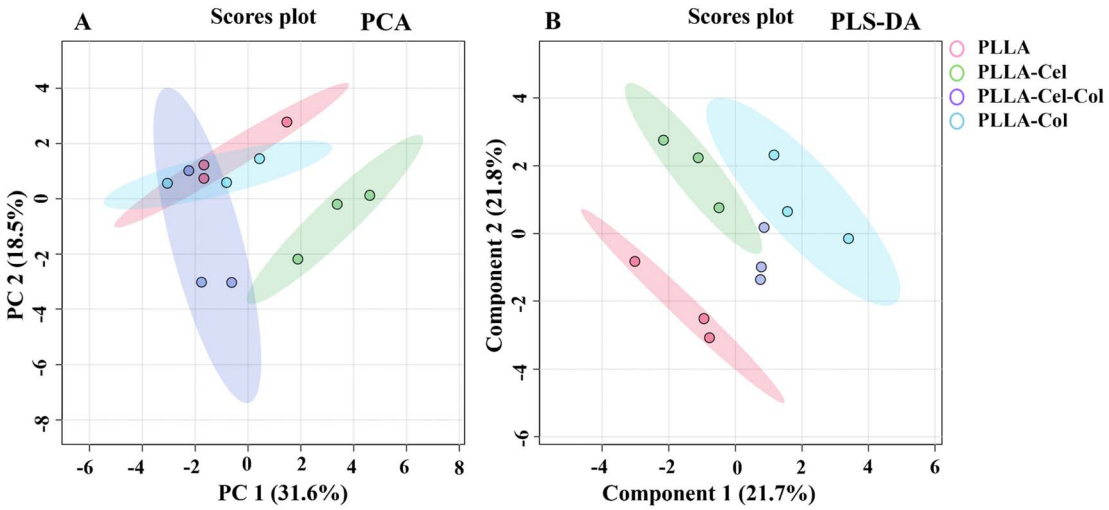

Fig. 2 Multivariate analyses of metabolomic profiles of MG63 cells cultured on PLLA and its composites, including PLLA-Cel, PLLA-Col, and PLLA-Cel-Col, for 7 days. Each data point represents a sample, with colors indicating the scaffold type: (A) principal component analysis (PCA) scores plot and (B) partial least-squares discriminant analysis (PLS-DA) scores plot.

Table 3 Variable importance in projection (VIP) scores from PLS-DA analysis

Metabolite	Component 1	Component 2
Succinic acid	2.3653	2.1663
3-Hydroxy-L-proline	2.0326	1.8647
Lactic acid	1.5342	1.3832
Proline	1.0615	1.15
Glucosylgalactosylhydroxylysine	1.0605	1.0792
FADH2	0.93318	1.1929
Glycylproline	0.84069	0.92553
Pyruvic acid	0.72669	0.87607
NADH	0.70272	0.69921
3-Phosphoglyceric acid	0.62646	0.65753
5-Hydroxylysine	0.46729	0.47517
cAMP	0.46231	0.70662
α-Ketoglutaric acid	0.31786	0.33859
Phosphoenol pyruvic acid	0.26945	0.3122
2-Phosphoglyceric acid	0.18599	0.16846
Oxaloacetic acid	0.13407	0.42237
Acetyl-CoA	0.1004	0.51071
Lysine	0.08856	0.23764

enrichment ratios and significant levels ($p < 0.05$). False discovery rate (FDR) adjustment was applied, and the highest-ranked 25 metabolic pathways were analyzed statistically (FDR-adjusted $p < 0.05$) to uncover a multifaceted metabolic reprogramming landscape. The D-amino acid metabolism pathway exhibited the maximal enrichment ratio of 2.5 ($p < 0.05$). Likewise, the lysine degradation pathway had an enrichment ratio of 2.0 ($p < 0.05$), confirming the bioactivity of the different scaffolds based on our primary research focused on bone tissue regeneration and, also, lysine's significant role in collagen biosynthesis.

3.4. Validation of lysine degradation for the promotion of bone formation in MG63 cells

Even though the D-amino acid metabolism was suggested to be the most significant pathway and had the highest enrichment ratio, we chose to validate the lysine degradation pathway instead, due to the complexity and specificity of the metabolic pathways. L-lysine was supplemented into the cell culture medium at different concentrations (50–400 μM).

Supplementation with L-lysine promoted bone formation processes, as shown by the significant enhancement in the alkaline phosphatase activity, collagen production and degree of calcification without alteration of the total protein content. The total protein content increased from day 4 to day 7, regardless of L-lysine supplementation. However, there was no significant difference in protein content among the groups with different concentrations of L-lysine supplementation at both time points (Fig. 4).

Specific ALP activity (Fig. 5), which is normalized to total protein content, exhibited a unique response to the L-lysine concentration. Specific ALP activity clearly increased between days 4 and 7 of culturing. Even though the role of L-lysine supplementation was insignificant on day 4, significant differences in the specific ALP activities at all L-lysine supplementation concentrations were clearly observed on day 7 when compared with the control without L-lysine supplementation ($p < 0.05$).

L-lysine had no effect on the collagen deposition level on day 4 of culturing, while on day 7, only supplementation with L-lysine at 400 μM showed significantly different collagen deposition ($p < 0.05$) (Fig. 6).

Likewise, L-lysine had no effect on mineralization on day 4 of culturing but it had significant effects on day 7 of the culture process (Fig. 7). Consistent with ALP activity, L-lysine supplementation at a concentration of 100 μM or higher had

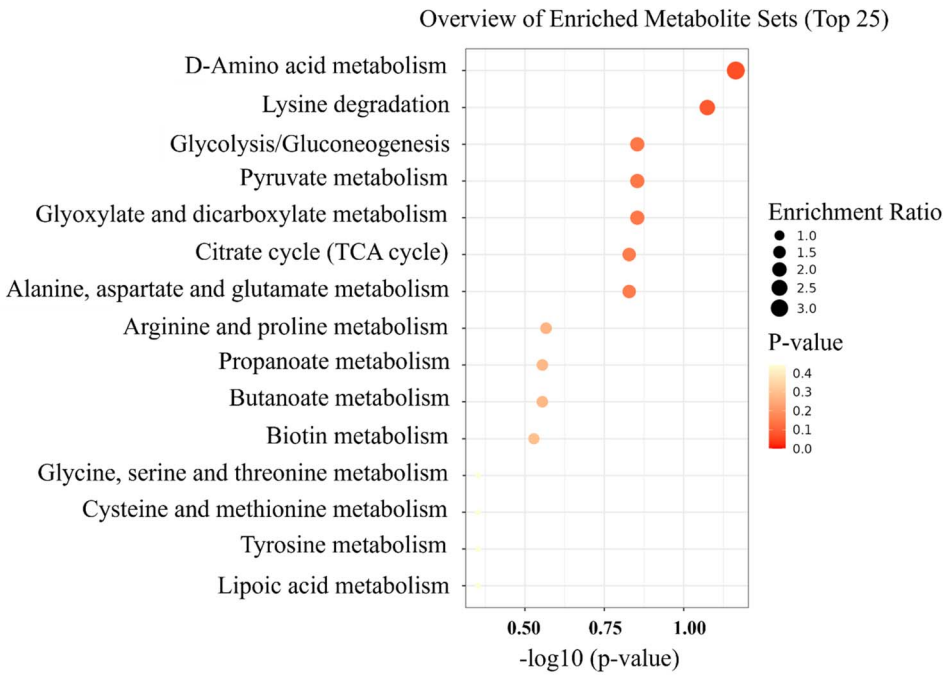

Fig. 3 Metabolic pathway enrichment analysis of MG63 cells cultured on PLLA, PLLA-Cel, PLLA-Col, and PLLA-Cel-Col for 7 days.

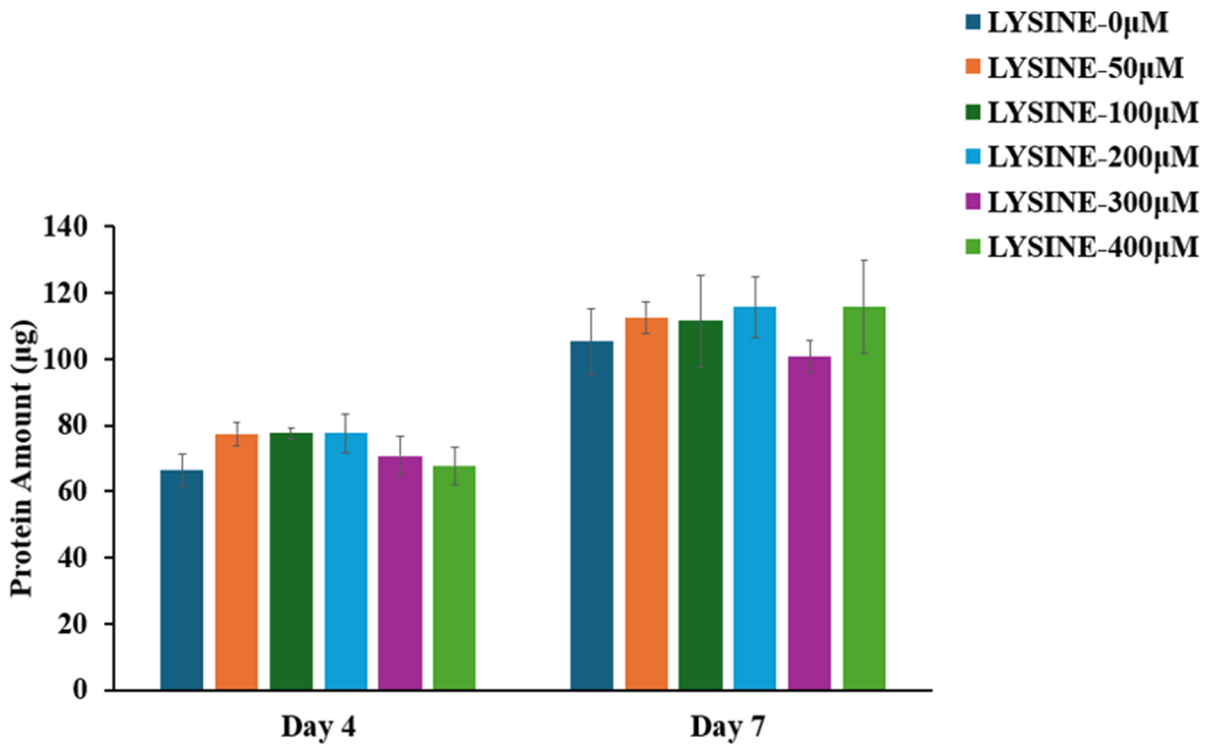

Fig. 4 Effect of L-lysine concentration on total protein content in MG63 osteoblast-like cells.

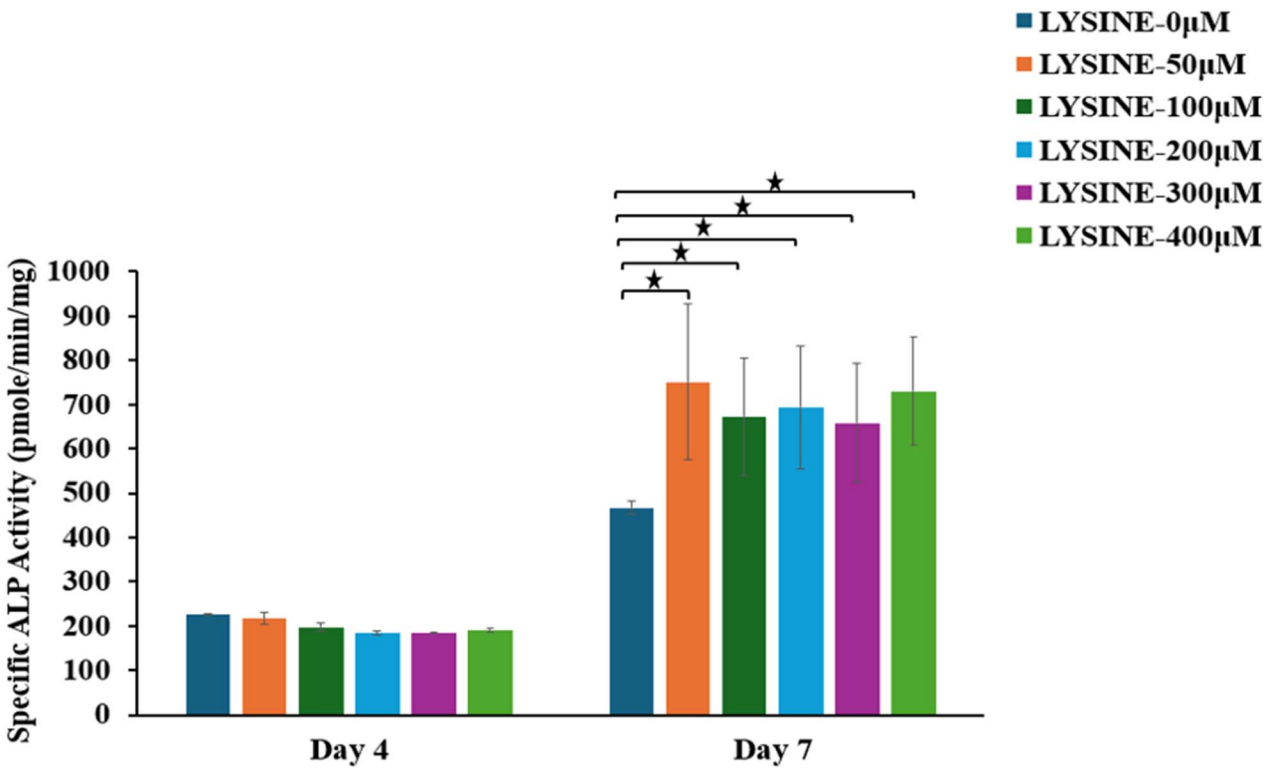

Fig. 5 Specific ALP activity normalized to the total protein content. L-lysine enhances alkaline phosphatase activity, a marker for osteogenic differentiation. The presented data are mean ± SD from triplicates of representative experiments, and the paired bars indicate a comparison of means. The star icon (★) indicates statistical significance when $p < 0.05$.

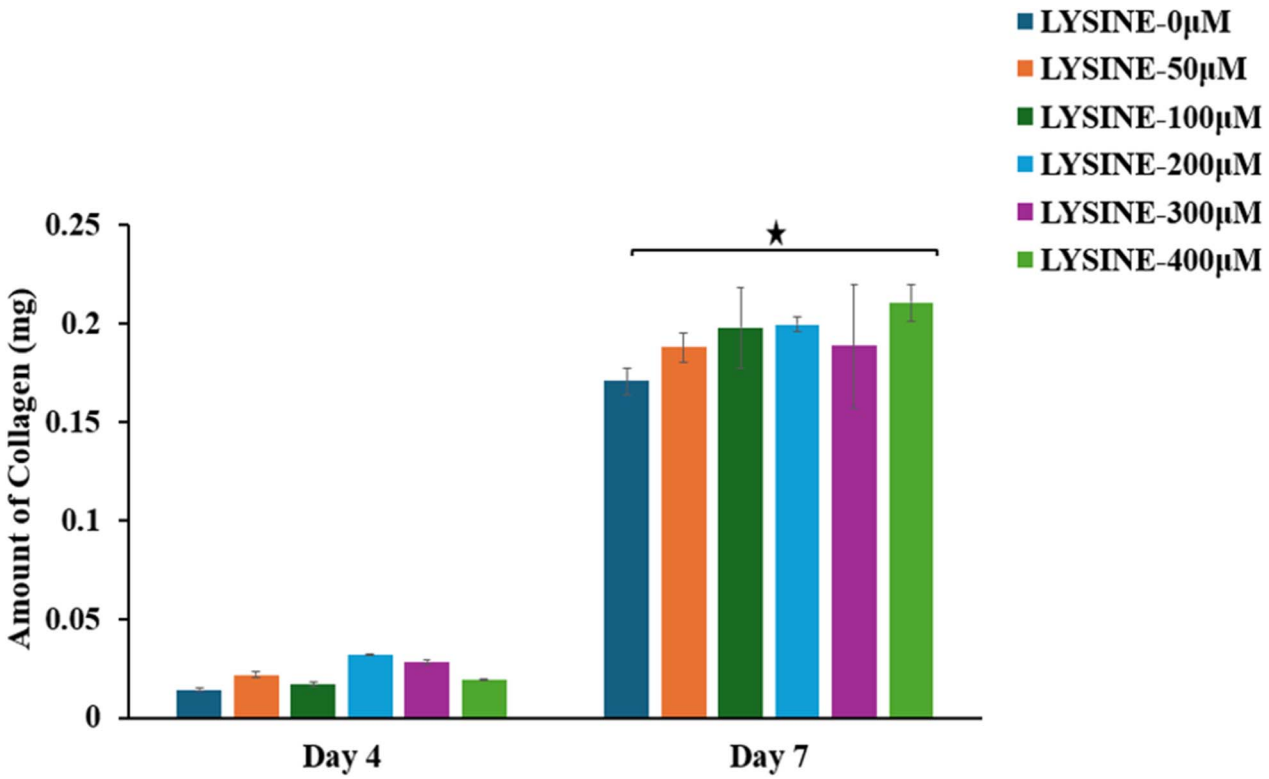

Fig. 6 L-lysine supplementation promotes collagen deposition. The presented data are mean ± SD from triplicates of representative experiments and the paired bars indicate a comparison of means. The star icon (★) indicates statistical significance when $p < 0.05$.

a significant effect on mineralization, as clearly observed on day 7, with the most significant mineralization occurring at 400 μM when compared with the control without L-lysine supplementation ($p < 0.05$).

3.5. Quantification of metabolites in the lysine degradation pathway

L-lysine is known to be degraded by reduction along with α-ketoglutarate, with saccharopine and α-aminoadipic acid being subsequently generated (Fig. 8A). The concentrations of lysine, saccharopine and α-aminoadipic acid were calculated from MG63 cells cultured on PLLA, PLLA-Cel, PLLA-Col, and PLLA-Cel-Col scaffolds (Fig. 8B). The analysis revealed distinct concentration profiles for saccharopine, α-aminoadipic acid, and lysine across the different scaffold compositions. Lysine concentrations ranged from ~10 μM to ~200 μM, with the highest concentration observed on the PLLA-Col scaffold and the lowest on the PLLA-Cel-Col scaffold. Saccharopine concentrations exhibited a range from ~20 μM to ~500 μM, with the highest concentration observed on the PLLA scaffold and the lowest on the PLLA-Cel-Col scaffold. α-Aminoadipic acid concentrations ranged from ~40 μM to ~400 μM, with the highest concentration observed on the PLLA-Col scaffold and the lowest on the PLLA-Cel-Col scaffold.

4. Discussion

The present research provides an integrated investigation into the metabolic and biological behaviors of MG63 cells on PLLA and composite scaffolds, more specifically focusing on scaffold composition and lysine metabolism. These metabolomic and biological activity data presented together suggested that there is a complex interaction between the materials and cellular metabolism and, ultimately, fundamental cellular functions.[30,31]

4.1. The influence of metabolomic landscape and scaffold composition on multivariate analysis

Metabolomics has increasingly been recognized as a powerful tool in tissue engineering research, offering insights into biochemical responses at a systems level.[16,17] In our study, ^{1}H-NMR-based metabolomics was used to provide a targeted and reproducible approach to profiling differential metabolic changes at the interface of scaffolds and MG63 cells.[18,32,33] The integration of PCA and PLS-DA sought to offer complementary perspectives: PCA can capture broad patterns of differential metabolite variation, while PLS-DA can enhance discrimination by leveraging class information.[34,35] Taken together, multivariate analysis revealed the significant influence of scaffold composition on shaping the metabolic landscape of MG63 cells, with particular emphasis on energy metabolism and collagen biosynthesis.

Multivariate analysis of differential metabolites obtained from MG63 cells cultured on PLLA and its composites revealed diverse differential metabolic responses influenced by scaffold composition. PCA demonstrated partial separation among the different scaffold groups, with the first two principal

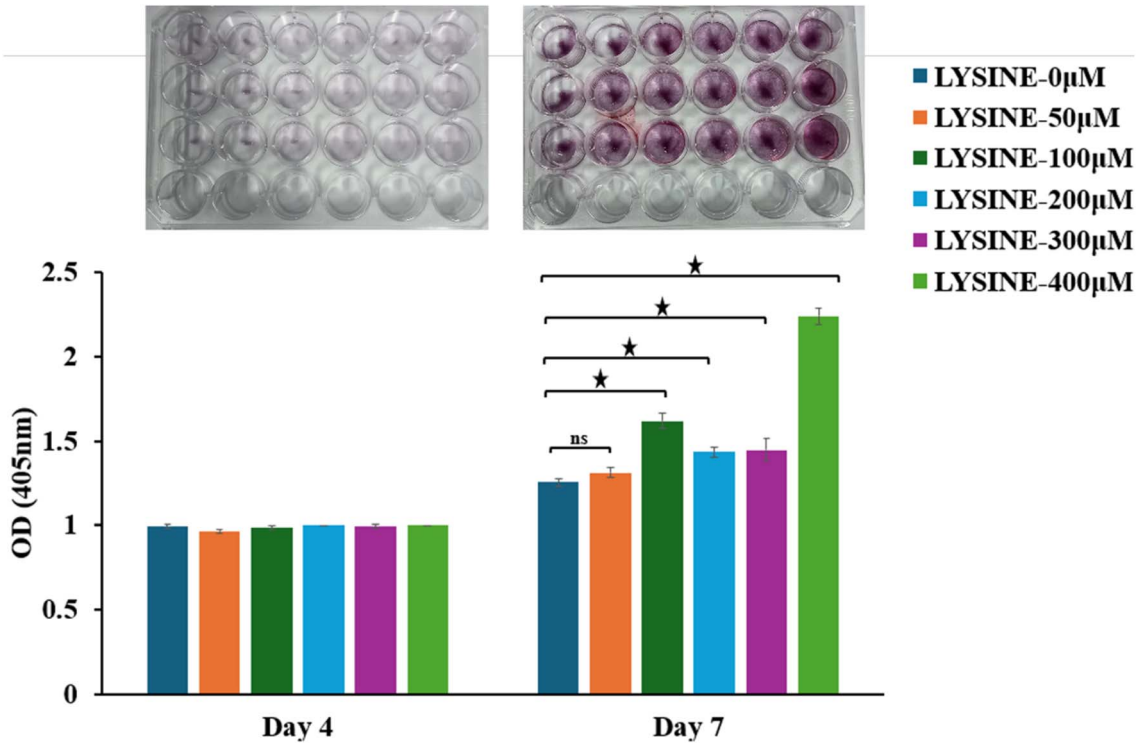

Fig. 7 Mineralization assessment by Alizarin Red S staining; the inset images are representative images of stained cells demonstrating calcium deposition in 24-well plates 4 and 7 days post-culture. The presented data are mean ± SD from triplicates of representative experiments and the paired bars indicate a comparison of means. The star icon (★) indicates statistical significance when $p < 0.05$, while "ns" denotes no significant difference.

components accounting for 31.6% and 18.5% of the total variance, respectively. This suggested that while there were observable differences in the metabolic signatures of cells grown on different scaffolds, a degree of overlap remained, likely due to shared metabolic pathways, similarities in scaffold compositions or conserved cellular functions across conditions.[31] Pairwise PERMANOVA comparisons further contextualized these observations, showing varying degrees of dissimilarity between scaffold types. Remarkably, although several comparisons exhibited high R^2 values explaining significant proportions of variance, none reached statistical significance. These findings suggested that while the material

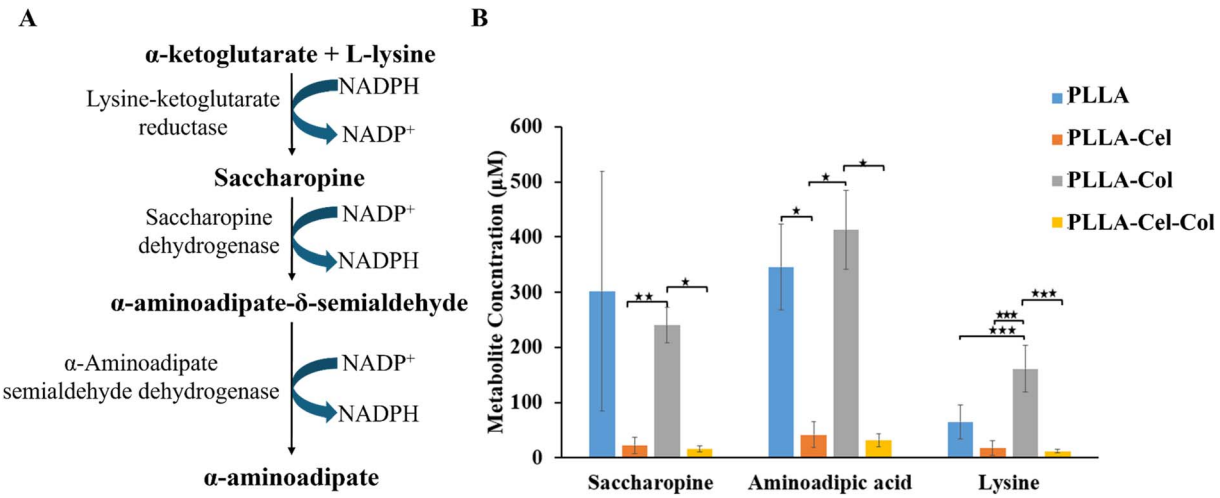

Fig. 8 Selected metabolites in the lysine degradation pathway. (A) The initial steps of the lysine degradation pathway and (B) the metabolite concentrations from MG63 cells cultured on PLLA, PLLA-Cel, PLLA-Col, and PLLA-Cel-Col for 7 days. The bar graph illustrating the mean ± SD ($n = 3$) of each metabolite concentration (μM) is derived from ^{1}H NMR metabolomic data. The paired bars indicate a comparison of means; (★) and (★★), and (★★★) indicate significant differences when $p < 0.05$, 0.01, and 0.001, respectively.

composition may influence cellular metabolism, the observed effects may not be strong enough to overcome biological variability within the current experimental design.[31]

PLS-DA, a supervised method, provided enhanced group discrimination, with VIP scores identifying the key metabolites driving group separation. Succinic acid, a central intermediate in the tricarboxylic acid (TCA) cycle, was consistently the most influential metabolite across all components, suggesting that mitochondrial activity and energy metabolism were significantly affected by scaffold composition. This was aligned with previous reports linking TCA cycle intermediates to osteogenic differentiation and matrix mineralization.[36,37] Similarly, 3-hydroxy-L-proline and glucosylgalactosylhydroxylysine, both collagen-specific post-translational modifications, were identified as important variables, reinforcing the hypothesis that collagen-containing scaffolds enhance extracellular matrix production and maturation.[38,39]

Interestingly, lactic acid, a marker of anaerobic glycolytic metabolism, revealed increased VIP scores on some scaffold types, highlighting a potential shift toward anaerobic metabolism in response to certain scaffold compositions, particularly PLLA-Cel scaffolds. While this could indicate a shift in oxygen availability or scaffold-induced changes in metabolic preference, it also highlighted the importance of understanding how biomaterials modulate energy metabolism in relation to cellular function.[40,41] The presence of $FADH_2$ and NADH as key electron carriers in oxidative phosphorylation further supported the idea that mitochondrial activity was influenced by scaffold composition.[37]

Another limitation of metabolomics analysis is the lack of absolute quantification of each metabolite, regardless of the method used. NMR-based metabolomics methods relying on the HMDB database, along with TSP internal standardization, are still widely used in targeted approaches where the metabolites of interest are already known prior to analysis. Nagana Gowda and Raftery (2019) suggested that NMR spectroscopy produces "inherently quantitative data without the need for compound-specific standards and is particularly well-suited for comparative metabolomics studies where relative changes in metabolite concentrations are of primary interest".[16] Araújo *et al.* (2019) used NMR metabolomics to analyze osteoblast reactions to PLLA to provide insights into cell metabolism in response to biomaterials.[19] This method could potentially save huge amounts during absolute quantification analyses in which different concentrations of known standards must be purchased at relatively high cost when thousands of metabolites require validation.

4.2. Enrichment analysis of differential metabolites

The enrichment analysis of differential metabolite sets was used to provide valuable insights into the metabolic pathways that could significantly alter the response to experimental conditions, especially the influence of the PLLA scaffold and its composite scaffolds. This analysis helped elucidate the underlying metabolic shifts associated with cellular responses to these biomaterials, offering a systems-level understanding of how scaffold composition influences metabolism.

The lysine degradation pathway was prominently enriched, with a high enrichment ratio and a significant *p*-value. This suggested that the incorporation of bioactive additives such as cellulose and collagen influenced the catabolism of lysine, potentially impacting protein synthesis and matrix production. Lysine is a crucial amino acid for collagen biosynthesis, and its degradation intermediates (*e.g.*, saccharopine and aminoadipic acid) were quantified to further support the relevance of this pathway in osteogenic differentiation.[8] Glycolysis/gluconeogenesis was another highly enriched pathway, indicating that energy metabolism is significantly influenced by the scaffold composition. This aligned with previous studies showing that a flux in glycolysis could regulate cell proliferation and differentiation, particularly in the hypoxic or nutrient-limited environments that are typical of tissue engineering scaffolds.[40,41] The observed trends in lactic acid levels, a glycolytic intermediate, across different scaffolds further supported this finding.

Pyruvate metabolism showed moderate enrichment, reflecting the relationship between glycolysis and the tricarboxylic acid (TCA) cycle. Pyruvate serves as a central node linking these pathways, and its metabolism influences both energy production and the anaplerotic reactions essential for biosynthesis. The elevated succinic acid levels observed in multivariate analysis reinforced the activation of pyruvate metabolism and downstream pathways. The TCA cycle was moderately enriched, suggesting oxidative phosphorylation and mitochondrial activity in response to certain scaffolds. This was consistent with the high VIP scores for succinic acid in the PLS-DA analysis, which highlighted the importance of the TCA cycle for distinguishing between scaffold types. Enhanced TCA cycle activity could indicate increased energy production and redox regulation, critical for osteoblast function and matrix deposition.[35]

Alanine, aspartate, and glutamate metabolism pathways showed moderate enrichment as well, which reflected the interrelation of amino acid metabolism and energy production. These amino acids serve as key intermediates in nitrogen metabolism and play key roles in maintaining cellular homeostasis. Their enrichment suggested that the biomaterials influenced amino acid utilization, potentially affecting protein synthesis and signaling pathways.[30,42] Arginine and proline metabolism were also enriched, indicating the modulation of pathways involved in nitric oxide production and collagen biosynthesis. Proline is a critical component of collagen, and its metabolism is closely linked to extracellular matrix formation.[38,39] The observed changes in proline levels and collagen production further validated the enrichment of this pathway.

The enrichment of specific metabolic pathways provided mechanistic insights into how the different scaffold compositions influence cellular behavior. Lysine degradation, pyruvate metabolism, and citrate cycle pathway enrichment suggested that the composite scaffolds (especially those containing collagen) promoted osteogenic differentiation by enhancing energy metabolism and collagen biosynthesis. Collagen-specific metabolites such as 3-hydroxy-L-proline and glucosylgalactosylhydroxylysine were identified as key contributors to group separation in the PLS-DA analysis, reinforcing the role of these pathways in matrix production.[38,39]

4.3. Biological activities and metabolic modulation validating lysine degradation

L-lysine is a critical component of cellular growth and metabolism. The elevated protein content suggested that L-lysine supplementation promoted cell proliferation and metabolic activity, which are critical steps in tissue regeneration. This assay finding directly links lysine availability to cellular function, providing a quantitative measure of the biomaterial's influence on cellular health and viability.[8]

Research by Torricelli *et al.* reveals that lysine treatment increases osteoblast proliferation and viability in rat femoral cultures.[26] It also appears that lysine enhances cell adhesion *via* increasing cationic surface sites, which aid in integrin binding and cytoskeletal remodeling. In our evaluation, the total protein content considerably increased on both days 4 and 7, indicating improved cell attachment and metabolic activity. Although no direct cell counting or viability experiments were performed during this phase, the increase in protein content is consistent with earlier research indicating that lysine stimulates osteoblast spreading, proliferation, and early-stage matrix formation.[43] This suggests that lysine supplementation promotes osteoblastic activity, even in the absence of physical scaffolding.

Lysine acts as a precursor for hydroxylysine, which aids in the development of permanent crosslinks between collagen molecules. This process is crucial for the formation of a mature extracellular matrix (ECM), which serves as a template for mineral deposition and maintains mechanical integrity.[44] In our investigation, the collagen content levels revealed an increase in collagen formation with increasing L-lysine concentration, especially on day 7. This is consistent with previous studies demonstrating that lysine-modified biomaterials improved collagen expression and matrix architecture.[44] Our findings support the hypothesis that lysine availability alone, without a scaffold effect, can enhance collagen formation, most likely *via* increased hydroxylysine cross-linking and better collagen stability.

According to Korbut *et al.*, lysine-modified scaffolds promote osteoblast development and matrix remodeling by increasing pro-inflammatory cytokine levels, such as IL-1β, IL-6, and TNF-α.[44] Although cytokine profiles were not examined under the current experimental conditions, the observed increases in ALP activity and collagen production suggest that lysine may have indirectly stimulated signaling pathways associated with osteogenic differentiation. Our results showed that lysine supplementation alone, without scaffold interactions, could activate osteogenic gene expression indicators, as evidenced by functional experiments. This lends credence to the concept that lysine possesses intrinsic osteoinductive capabilities, and it could be employed as a bioactive supplement in bone regeneration procedures, either in conjunction with scaffolds or in scaffold-free contexts, such as injectable systems or *in vivo* delivery methods.

Mineralization is determined not just by calcium availability but also by the quality and structure of the collagenous matrix. Lysine-derived hydroxylysine residues play a vital role in forming hydroxyapatite crystal nucleation sites.[44] Collagen fibers cannot adequately bind calcium if lysine levels are low, which impairs mineral deposition. Calcium deposition in our evaluation was time dependent. This pattern highlights the importance of lysine for generating an appropriate ECM structure, which allows for successful mineralization. The delayed peak in mineralization compared to ALP activity shows that lysine supports early differentiation and collagen production before impacting mineralization, as previously seen in osteoblast cells.[8,45]

4.4. Effects of biomaterial components and metabolic changes leading to bone formation

While our study was based on the results from triplicate analysis of each material type, it was still large enough for data analysis. Our triplicate result analysis was consistent with preliminary metabolomics studies by Araújo and colleagues in which the metabolites of human osteoblasts grown on non-poled and poled poly(L-lactic) acid were measured at different time points and in triplicate at each time point.[19] The increase in aminoadipic acid supported the hypothesis that collagen-containing scaffolds modulate lysine metabolism, potentially enhancing energy production and redox balance through the TCA cycle intermediates derived from this pathway.[45]

The observed trend in lysine degradation metabolites, particularly the considerable drop in metabolite concentrations on cellulose-containing scaffolds (PLLA-Cel and PLLA-Cel-Col), may be attributed to changes in mechanical reinforcement and surface chemistry imparted by cellulose, as noted in a previous study on cellulose-based composites for bone tissue engineering.[46] These reductions could also be attributed to the physicochemical properties of these scaffolds, particularly their glass transition temperature (T_g), cold crystallization enthalpy (ΔH_{cc}), tensile strength, Young's modulus, and weight loss after simulated body fluid (SBF) immersion, as detailed in our previous report. Understanding how these physical traits relate to metabolic responses gives vital insights into the interaction between material properties and cellular function. One significant observation from our previous investigation was that the T_g values of PLLA-Cel and PLLA-Cel-Col were somewhat higher than those of pure PLLA and PLLA-Col, and the lower value of PLLA-Cel ΔH_{cc} indicated enhanced stiffness and decreased polymer chain mobility as a result of cellulose inclusion due to reduced amorphous content[47] and surface chemistry modifications.[46] This increased stiffness could impact cell adhesion, metabolism, differentiation and spreading, altering metabolic activity, as reported in a previous study.[48] The lower quantities of saccharopine, aminoadipic acid, and lysine on cellulose-containing scaffolds may represent this change in cellular energy allocation.

Furthermore, the reduced levels of lysine catabolic products on cellulose-containing scaffolds could suggest a possible change in cellular metabolism away from catabolic activities and toward anabolic pathways such as protein synthesis and extracellular matrix (ECM) formation.[47] This could imply that more lysine may be accessible for incorporation into structural proteins, hence promoting matrix deposition and tissue

development. Cellulose, while not intrinsically osteoinductive, may serve as a source of bioactive signals that alter cellular function, such as providing surface-bound functional groups (*e.g.*, hydroxyl groups) or supporting minor variations in local pH and ion exchange. Should cellulose-containing scaffolds modify the metabolic landscape of MG63 cells and favour matrix synthesis over amino acid degradation, this could imply that the presence of cellulose sends biochemical signals that regulate cellular function.[46]

In yet another study, researchers found that acetylation of bacterial cellulose increases hemocompatibility, protein adsorption, and 3D cell development while maintaining mechanical integrity. The scaffolds facilitated cell adhesion and proliferation *in vitro*, resulting in enhanced metabolic activity over time, as seen in MTT assay findings. These findings imply that changes such as acetylation not only improved the scaffold's physical robustness but also established a conducive environment for long-term cellular metabolism. This is consistent with our findings, in which cellulose-containing scaffolds (PLLA-Cel and PLLA-Cel-Col) showed decreased lysine degradation, indicating a shift toward matrix synthesis rather than catabolic pathways. The improved surface topography and mechanical strength supplied by cellulose may affect integrin-mediated signaling and cytoskeletal remodeling, supporting anabolic processes like collagen formation and extracellular matrix deposition.[12,49]

5. Conclusions

This study shows that the composition of PLLA-based scaffolds has a considerable impact on the metabolic activity of MG63 osteoblast-like cells, notably in connection to the lysine degradation pathway. Using ^{1}H-NMR-based metabolomics and multivariate analysis, we discovered distinct metabolic signatures among the scaffold types, with PLLA-Col scaffolds exhibiting elevated levels of lysine-derived metabolites associated with extracellular matrix synthesis and osteogenesis.

The incorporation of cellulose and collagen into PLLA scaffolds improves surface characteristics and mechanical performance and fosters a cellular metabolic environment favorable for bone formation. Bioactivity experiments demonstrated that L-lysine supplementation increased collagen synthesis and mineralization, particularly at 400 μM after 7 d of culturing. These findings imply that lysine metabolism is an important biochemical indication of osteogenic capacity and may be used to optimize biomaterial design.

Our findings emphasize the necessity of taking a comprehensive approach to studying scaffold–cell interactions using metabolomics, providing fresh insights into how the material composition might influence metabolic reprogramming. By identifying lysine degradation as a key route influenced by scaffold type, we provide the groundwork for future research into the molecular processes driving these metabolic alterations and their effects on osteogenesis. Further research should look at the *in vivo* validation of these findings to determine the long-term impact of scaffold-induced metabolic modulation on bone repair.

This study adds to our expanding understanding of how biomaterials affect cellular metabolism and emphasizes the need to combine metabolic profiling with functional tests in bone tissue engineering procedures. The ability to relate scaffold composition to particular metabolic responses opens up new possibilities for developing more effective biomaterials that enhance osteogenic outcomes *via* targeted metabolic control.

Author contributions

Conceptualization: Z. Z., B. T., C. J., J. R.; methodology: Z. Z., Z. L., B. T., V. C., D. B., G. K., C. J.; formal analysis: Z. Z., C. J., G. K., J. R.; investigation: Z. Z., Z. L., B. T., V. C., D. B., G. K., C. J.; visualization: Z. Z., G. K.; data curation; Z. Z., J. R., C. J.; funding acquisition: Z. Z., J. R.; supervision: C. J., B. T., V. C., D. B., J. R.; project administration: J. R.; writing-original draft: Z. Z., J. R.; writing-review and editing: Z. Z., C. J., B. T., V. C., D. B., J. R.

Conflicts of interest

The authors declare no conflicts of interest.

Data availability

This study was carried out using publicly available data from **https://www.hmdb.ca/**. Also, data for this article are available at **https://drive.google.com/drive/folders/1yoWjssqzVGJ_4IsIZR6XxcNxWMBuIpw5?usp=sharing**.

Acknowledgements

This research project was partially supported by Fundamental Fund 2022, Chiang Mai University. Also, partial support was obtained from the Faculty of Medicine Chiang Mai University. This research was partially supported by Chiang Mai University. In addition, the Presidential Scholarship also contributed to supporting living expenses and the tuition fee for the student who is the first author for his PhD program in Biochemistry.

References

1 P. Saini, M. Arora and M. N. V. R. Kumar, Poly(lactic acid) blends in biomedical applications, *Adv. Drug Delivery Rev.*, 2016, **107**, 47–59.
2 L. Xiao, B. Wang, G. Yang and M. Gauthier, in *Biomedical Science, Engineering and Technology*, ed. D. N. Ghista, InTech, Rijeka, 2012, ch. 13, pp. 247–282.
3 A. Grémare, V. Guduric, R. Bareille, V. Heroguez, S. Latour, N. L'heureux, *et al.*, Characterization of printed PLA scaffolds for bone tissue engineering, *J. Biomed. Mater. Res., Part A*, 2018, **106**(4), 887–894.
4 L. I. Vayshbeyn, E. E. Mastalygina, A. A. Olkhov and M. V. Podzorova, Poly(lactic acid)-Based Blends: A Comprehensive Review, *Appl. Sci.*, 2023, **13**(8), 5148.
5 A. Leonés, L. Peponi, M. Lieblich, R. Benavente and S. Fiori, In Vitro Degradation of Plasticized PLA Electrospun Fiber

Mats: Morphological, Thermal and Crystalline Evolution, *Polymers*, 2020, **12**(12), 2975.

6 Z. Ziblim, B. Thapsukhon, V. Choommongkol, D. Boonyawan, K. Inthanon, O. Khantamat, *et al.*, Collagen-cellulose-poly(l-lactide) scaffold by electrospinning and plasma-assisting fabrication for bone tissue engineering applications, *Plasma Processes Polym.*, 2024, **21**(6), 2300209.

7 X. Hu, T. Wang, F. Li and X. Mao, Surface modifications of biomaterials in different applied fields, *RSC Adv.*, 2023, **13**(30), 20495–20511.

8 J. Feng, D. Zhang, M. Zhu and C. Gao, Poly(l-lactide) melt spun fiber-aligned scaffolds coated with collagen or chitosan for guiding the directional migration of osteoblasts in vitro, *J. Mater. Chem. B*, 2017, **5**(26), 5176–5188.

9 C. A. Murphy and M. N. Collins, Microcrystalline cellulose reinforced polylactic acid biocomposite filaments for 3D printing, *Polym. Compos.*, 2018, **39**(4), 1311–1320.

10 M. Mohammadalipour, S. Karbasi, T. Behzad, Z. Mohammadalipour and M. Zamani, Effect of cellulose nanofibers on polyhydroxybutyrate electrospun scaffold for bone tissue engineering applications, *Int. J. Biol. Macromol.*, 2022, **220**, 1402–1414.

11 K. M. N'Gatta, H. Belaid, J. El Hayek, E. F. Assanvo, M. Kajdan, N. Masquelez, *et al.*, 3D printing of cellulose nanocrystals based composites to build robust biomimetic scaffolds for bone tissue engineering, *Sci. Rep.*, 2022, **12**(1), 21244.

12 P. K. Szewczyk, K. Berniak, J. Knapczyk-Korczak, J. E. Karbowniczek, M. M. Marzec, A. Bernasik, *et al.*, Mimicking natural electrical environment with cellulose acetate scaffolds enhances collagen formation of osteoblasts, *Nanoscale*, 2023, **15**(15), 6890–6900.

13 A. M. Pandele, A. Constantinescu, I. C. Radu, F. Miculescu, S. Ioan Voicu and L. T. Ciocan, Synthesis and Characterization of PLA-Micro-structured Hydroxyapatite Composite Films, *Materials*, 2020, **13**(2), 274.

14 F. Boccafoschi, L. Fusaro, C. Mosca, M. Bosetti, P. Chevallier, D. Mantovani, *et al.*, The biological response of poly(L-lactide) films modified by different biomolecules: Role of the coating strategy, *J. Biomed. Mater. Res., Part A*, 2012, **100A**(9), 2373–2381.

15 Y. Zhu, K. S. Chian, M. B. Chan-Park, P. S. Mhaisalkar and B. D. Ratner, Protein bonding on biodegradable poly(l-lactide-co-caprolactone) membrane for esophageal tissue engineering, *Biomaterials*, 2006, **27**(1), 68–78.

16 G. A. Nagana Gowda and D. Raftery, in *NMR-Based Metabolomics*, ed. G. A. N. Gowda and D. Raftery, Springer, New York, 2019, vol. 2037, pp. 3–14.

17 G. A. Nagana Gowda and D. Raftery, in *Cancer Metabolomics*, ed. S. Hu, Springer International Publishing, Cham, 2021, vol. 1280, pp. 19–37.

18 M. H. Baky, I. M. Kamal, L. A. Wessjohann and M. A. Farag, Assessment of metabolome diversity in black and white pepper in response to autoclaving using MS- and NMR-based metabolomics and in relation to its remote and direct antimicrobial effects against food-borne pathogens, *RSC Adv.*, 2024, **14**(15), 10799–10813.

19 R. Araújo, T. J. Carneiro, P. Marinho, M. M. da Costa, A. Roque, O. A. B. da Cruz e Silva, *et al.*, NMR metabolomics to study the metabolic response of human osteoblasts to non-poled and poled poly (L-lactic) acid, *Magn. Reson. Chem.*, 2019, **57**(11), 919–933.

20 J. Fan, V. Jahed and K. Klavins, Metabolomics in Bone Research, *Metabolites*, 2021, **11**(7), 434.

21 G. Scoponi, N. Francini and A. Athanassiou, Production of Green Star/Linear PLA Blends by Extrusion and Injection Molding: Tailoring Rheological and Mechanical Performances of Conventional PLA, *Macromol. Mater. Eng.*, 2021, **306**(5), 2000805.

22 P. Somtua, C. Jaikang, G. Konguthaithip, K. Intui, S. Watcharakhom, T. E. O'Brien, *et al.*, Postmortem Alteration of Purine Metabolism in Coronary Artery Disease, *Metabolites*, 2023, **13**(11), 1135.

23 M. Matsuda and Y. Asano, Determination of plasma and serum l-lysine using l-lysine ε-oxidase from Marinomonas mediterranea NBRC 103028T, *Anal. Biochem.*, 2010, **406**(1), 19–23.

24 E. V. Butorov, Relationship between plasma l-lysine concentrations and levels of HIV-1 RNA, *Virulence*, 2013, **4**(7), 646–653.

25 M. Yoshikawa, Y. Shimomura, H. Kakigi, N. Tsuji, T. Yabuuchi and H. Hayashi, Effect of L-lysine in culture medium on nodule formation by bone marrow cells, *J. Biomed. Sci. Eng.*, 2012, **05**(10), 587–592.

26 P. Torricelli, M. Fini, G. Giavaresi and R. Giardino, Bone tissue cultures: An *in vitro* model for the evaluation of bone defect healing after L-arginine and L-lysine administration, *Artif. Cells, Blood Substitutes, Immobilization Biotechnol.*, 2001, **29**(4), 325–334.

27 M. Fini, P. Torricelli, G. Giavaresi, A. Carpi, A. Nicolini and R. Giardino, Effect of L-lysine and L-arginine on primary osteoblast cultures from normal and osteopenic rats, *Biomed. Pharmacother.*, 2001, **55**(4), 213–220.

28 P. Torricelli, M. Fini, G. Giavaresi, R. Giardino, S. Gnudi, A. Nicolini, *et al.*, L-Arginine and L-Lysine stimulation on cultured human osteoblasts, *Biomed. Pharmacother.*, 2002, **56**(10), 492–497.

29 S. W. Tsai, H. M. Liou, C. J. Lin, K. L. Kuo, Y. S. Hung, R. C. Weng, *et al.*, MG63 Osteoblast-Like Cells Exhibit Different Behavior when Grown on Electrospun Collagen Matrix *versus* Electrospun Gelatin Matrix, *PLoS One*, 2012, **7**(2), e31200.

30 C. H. Johnson, J. Ivanisevic and G. Siuzdak, Metabolomics: beyond biomarkers and towards mechanisms, *Nat. Rev. Mol. Cell Biol.*, 2016, **17**(7), 451–459.

31 D. S. Wishart, Emerging applications of metabolomics in drug discovery and precision medicine, *Nat. Rev. Drug Discovery*, 2016, **15**(7), 473–484.

32 R. M. Gathungu, R. Kautz, B. S. Kristal, S. S. Bird and P. Vouros, The integration of LC-MS and NMR for the analysis of low molecular weight trace analytes in complex matrices, *Mass Spectrom. Rev.*, 2020, **39**(1–2), 35–54.

33 J. Figueira, S. Gouveia-Figueira, C. Öhman, P. Lif Holgerson, M. L. Nording and A. Öhman, Metabolite quantification by NMR and LC-MS/MS reveals differences between unstimulated, stimulated, and pure parotid saliva, *J. Pharm. Biomed. Anal.*, 2017, **140**, 295–300.
34 A. Teti, Mechanisms of osteoclast-dependent bone formation, *BoneKEy Rep.*, 2013, **2**, 449.
35 A. Mediani and S. N. Baharum, in *Systems Biology*, ed. M. Bizzarri, Springer US, New York, 2024, vol. 2745, pp. 77–90.
36 N. S. Chandel, Mitochondria as signaling organelles, *BMC Biol.*, 2014, **12**(1), 34.
37 I. Martínez-Reyes and N. S. Chandel, Mitochondrial TCA cycle metabolites control physiology and disease, *Nat. Commun.*, 2020, **11**(1), 102.
38 M. D. Shoulders and R. T. Raines, Collagen Structure and Stability, *Annu. Rev. Biochem.*, 2009, **78**(1), 929–958.
39 S. Ricard-Blum, The Collagen Family, *Cold Spring Harbor Perspect. Biol.*, 2011, **3**(1), a004978.
40 M. G. Vander Heiden, L. C. Cantley and C. B. Thompson, Understanding the Warburg Effect: The Metabolic Requirements of Cell Proliferation, *Science*, 2009, **324**(5930), 1029–1033.
41 M. V. Liberti and J. W. Locasale, The Warburg Effect: How Does it Benefit Cancer Cells?, *Trends Biochem. Sci.*, 2016, **41**(3), 211–218.
42 J. K. Nicholson and J. C. Lindon, Metabonomics, *Nature*, 2008, **455**(7216), 1054–1056.
43 Ł. Kaniuk, Z. J. Krysiak, S. Metwally and U. Stachewicz, Osteoblasts and fibroblasts attachment to poly(3-hydroxybutyric acid-co-3-hydrovaleric acid) (PHBV) film and electrospun scaffolds, *Mater. Sci. Eng. C*, 2020, **110**, 110668.
44 A. Korbut, M. Włodarczyk, K. Rudnicka, A. Szwed, P. Płocí Nski, M. Biernat, *et al.*, Three Component Composite Scaffolds Based on PCL, Hydroxyapatite, and L-Lysine Obtained in TIPS-SL: Bioactive Material for Bone Tissue Engineering, *Int. J. Mol. Sci.*, 2021, **22**, 13589, DOI: **10.3390/ijms222413589**.
45 M. E. Lacouture, J. L. Schaffer and L. B. Klickstein, A Comparison of Type I Collagen, Fibronectin, and Vitronectin in Supporting Adhesion of Mechanically Strained Osteoblasts, *J. Bone Miner. Res.*, 2002, **17**(3), 481–492.
46 M. Janmohammadi, Z. Nazemi, A. O. M. Salehi, A. Seyfoori, J. V. John, M. S. Nourbakhsh, *et al.*, Cellulose-based composite scaffolds for bone tissue engineering and localized drug delivery, *Bioact. Mater.*, 2023, **20**, 137–163.
47 I. G. R. da Silva, B. T. dos S. Pantoja, G. H. D. R. Almeida, A. C. O. Carreira and M. A. Miglino, Bacterial Cellulose and ECM Hydrogels: An Innovative Approach for Cardiovascular Regenerative Medicine, *Int. J. Mol. Sci.*, 2022, **23**(7), 3955.
48 J. Na, Z. Yang, Q. Shi, C. Li, Y. Liu, Y. Song, *et al.*, Extracellular matrix stiffness as an energy metabolism regulator drives osteogenic differentiation in mesenchymal stem cells, *Bioact. Mater.*, 2024, **35**, 549–563.
49 M. W. Ullah, F. Subhan, S. Manan, M. Ul-Islam, K. F. Alabbosh, T. Kamal, *et al.*, Impact of structural features of acetylated bacterial cellulose on cell-scaffold and scaffold-blood interactions in vitro, *Cellulose*, 2023, **30**(16), 10373–10399.